


1 **Neotectonic shortening and foreland structural evolution of the Malta Horst Cenozoic**
2 **carbonate succession, Central Mediterranean**

Author: Peter Gatt

Malta College of Arts, Science and Technology, Paola, Malta

 PG, 0000-0003-3871-8395

corresponding author email: pgatt.geo@gmail.com

3
4 **Abstract**

5
6 The Malta Horst is a NW-SE trending, 30 km-wide structural high situated on the southern
7 Hyblean-Malta Plateau, which is an African continental indenter in collision with Eurasia.
8 Sediments consist of a shallow marine carbonate platform succession (Mesozoic to
9 Oligocene) capped by Miocene pelagic carbonates and marl. Utilizing seismic profiles, well
10 data, and outcrop observations, this study provides the first description of kilometre-scale
11 contractional structures within the horst and analyses the reactivation of normal faults by
12 transcurrent movement under NW compression. The tectonic evolution of this foreland
13 region is defined by five distinct phases (A through E), alternating between extension and
14 compression. This cyclicity reflects the interplay between the migrating Calabrian Arc and the
15 converging African craton. Initial NE-SW trending faults (Phases A and B) developed during
16 the Late Oligocene to Early Miocene, coinciding with platform drowning. Following Tortonian
17 uplift (Phase C), accelerated migration of the Calabrian Arc during Phase D triggered N-S
18 extension, establishing the NW-SE and NE-SW normal faults that bound the Malta Horst. The
19 neotectonic regime (Phase E) marks a return to dominance of the NW-directed compression
20 by the African craton as the Calabrian Arc migration decelerated. This regional stress field has
21 reactivated the NW-SE marginal normal faults through strike-slip motion. The combination of
22 transcurrent drag and regional compression has inverted Phase A NE-SW normal faults into
23 oblique reverse faults. These thrusts sole along a weak top Eocene evaporite décollement,
24 producing a series of folds and inverted basins within 10 km of the horst's northeast margin.
25 Onshore, these structures are manifest as en echelon, non-cylindrical, and doubly plunging
26 folds that define the topography of Malta's northeast coast. These shear zone structures are
27 thin-skinned deformations in Oligo-Miocene sediments controlled by thick-skinned, W-E
28 transcurrent movement in the crust and Mesozoic sediments. Ongoing compression suggests
29 an increase in seismic risk proximal to the Maltese Islands, with significant implications for
30 local geohazard frequency and magnitude.

31

32

33 Résumé

34 Le Horst de Malte est un haut-fond structural de 30 km de large, orienté NO-SE, situé sur la
35 partie sud du plateau Hybléen-Maltaise, qui constitue un poinçon continental africain en
36 collision avec l'Eurasie. La sédimentation se compose d'une succession de plateforme
37 carbonatée marine peu profonde (du Mésozoïque à l'Oligocène), surmontée par des
38 carbonates pélagiques et des marnes du Miocène. En s'appuyant sur des profils sismiques,
39 des données de puits et des observations d'affleurements, cette étude fournit la première
40 description de structures de contraction à l'échelle kilométrique au sein du horst et analyse
41 la réactivation de failles normales par un mouvement transcurrent sous une compression NO.
42 L'évolution tectonique de cette région d'avant-pays est définie par cinq phases distinctes (A
43 à E), alternant entre extension et compression. Cette cyclicité reflète l'interaction entre la
44 migration de l'arc calabrais et la convergence du craton africain: Phases A et B (Oligocène
45 supérieur à Miocène inférieur); Développement des premières failles orientées NE-SO,
46 coïncidant avec l'ennoiement de la plateforme; Phase C (Tortonien), soulèvement tectonique;
47 Phase D, l'accélération de la migration de l'arc calabrais déclenche une extension N-S,
48 établissant les failles normales NO-SE et NE-SO qui délimitent le horst de Malte et, Phase E,
49 (régime néotectonique) marque le retour à la dominance de la compression dirigée vers le
50 NO par le craton africain, alors que la migration de l'arc calabrais ralentit. Ce champ de
51 contraintes régional a réactivé les failles normales marginales NO-SE par un mouvement de
52 décrochement. La combinaison de l'entraînement transcurrent et de la compression
53 régionale a inversé les failles normales NE-SO de la Phase A en failles inverses obliques. Ces
54 chevauchements s'enracinent le long d'un niveau de décollement ductile d'évaporites du
55 sommet de l'Éocène, produisant une série de plis et de bassins inversés à moins de 10 km de
56 la marge nord-est du horst. À terre, ces structures se manifestent par des plis en échelon, non
57 cylindriques et à double plongement, qui définissent la topographie de la côte nord-est de
58 Malte. Ces structures de zone de cisaillement sont des déformations de couverture (*thin-*
59 *skinned*) dans les sédiments oligo-miocènes, contrôlées par un mouvement transcurrent E-O
60 de socle (*thick-skinned*) dans la croûte et les sédiments mésozoïques. La compression actuelle
61 suggère une augmentation du risque sismique à proximité des îles maltaises, avec des
62 implications significatives pour la fréquence et l'ampleur des risques géologiques locaux.

63

64 **Keywords:** Maltese Islands, foreland, inversion tectonics, foreland, carbonate platforms.

65 **Mots-clés:** Îles maltaises, avant-pays, plissement en échelon, anticlinaux, plates-formes
66 carbonatées.

67

68

69

70 **1 Introduction**

71 The Late Cretaceous convergence of the African and Eurasian plates triggered the
72 development of several Mediterranean orogenic belts (Dewey et al., 1973; Rosenbaum &
73 Lister, 2004; van Hinsbergen et al., 2020a). The orogenic loading and migrating arcs have
74 downflexed the African foreland, with thick-skinned tectonics (Morticelli et al., 2015)
75 generating foreland extension perpendicular to the foredeep (Decelles & Giles, 1996). In the
76 Central Mediterranean, the Pelagian Block has been loaded by the Sicilian-Maghrebian
77 orogenic belt (Argnani, 1987; Butler et al., 1992; Corti et al., 2006; Maiorana et al., 2023).
78 Crustal inhomogeneity of the Pelagian foreland along the collisional front resulted in its
79 segmentation into three distinct blocks separated by N-S trending strike-slip faults (Ben-
80 Avraham et al., 1995):

81 1. The Hyblean-Malta Plateau (HMP): A trapezoidal-shaped, African continental indenter
82 bounded by three transcurrent faults: the Scicli Fault on the west, the Malta
83 Escarpment fault on the east and the Medina Wrench on the south (S1, S2 and S3 in
84 figure 1a). Owing to its relative thickness and buoyancy, the rigid crust resisted
85 significant subduction along the SE Sicilian collision front (Cowie & Kuszniir, 2012;
86 Gardiner et al., 1995), leading to the formation of oroclines along its margins (Ben-
87 Avraham et al., 1995; Rosenbaum, 2014).

88 2. The Gela Basin: Situated to the west of the HMP, this down-flexed basin is further
89 delimited in the western Sicily Channel by the seismically active Sciacca strike-slip fault
90 (Civile et al., 2021; Soumaya et al., 2015).

91 3. The Ionian Block: lies to the east of the Hyblean-Malta Plateau (HMP), divided by the
92 Malta Escarpment transform fault. Characterized by oceanic crust at depths exceeding
93 3 km, this block is subducting beneath the Calabrian Arc. Much of its structure is
94 obscured by a dense accretionary prism (Gutscher et al., 2017; Tugend et al., 2019).

95 GPS measurements in the Central Mediterranean show a NW-directed regional stress field,
96 driven by the 5 mm yr⁻¹ convergence of the African plate (Hollenstein et al., 2003; Serpelloni
97 et al., 2007). The stress has deformed the northern tip of the HMP indenter in SE Sicily (Cogan
98 et al., 1989; Pedley & Grasso, 1992) and generated strain about 150 km away from the
99 collision front, along the NW-SE trending, <30 km-wide Malta Horst (Fig. 1 b). Early-stage
100 deformation is characterized by the development of synthetic and antithetic shears, alongside
101 secondary synthetic strike-slip and normal faults (Tchalenko, 1970), producing a hierarchy of
102 first-, second-, and third-order strike-slip faults (Moody & Hill, 1956). The thin-skinned
103 shearing is associated with the underlying Principal Displacement Zone (PDZ), which is
104 characteristically oriented oblique to the maximum principal stress (σ_1) (Sylvester, 1988).
105 Sustained convergence results in thrust systems, often in en echelon arrangements and
106 shortening of existing intraplateform grabens by basin inversion (Bally, 1984; Bonini et al.,
107 2012; Zwaan et al., 2022). Deep-seated basement faults may seed this thin-skinned thrusting

108 and localized folding (Butler et al., 2025). Within these settings, low friction lithologies such
109 as evaporites, serve as critical décollement surfaces, facilitating the translation and folding of
110 the sedimentary cover (Letouzey et al., 1995).

111 This study describes the neotectonics of the Malta Horst area that entered a foreland position
112 since the Miocene (Dart et al., 1993; Maiorana et al., 2023). The Malta Horst is bounded by
113 a set of conjugate normal faults, the here named Sikka Fault and Hurd Bank Fault along its NE
114 margin and by the Maghlaq fault system (Bonson et al., 2007; Illies, 1981) along its SW margin.
115 The horst is adjacent to the >500 m deep Pantelleria Rift (Fig. 1 b) bounded by the Malta
116 Graben Fault which trends NW but makes a sharp change in direction to W-E south of Gozo
117 (East Malta Graben Fault). The Maltese Islands are the only subaerial part of the Malta Horst
118 (Fig. 1 c) located along the northern margin of the 200 km-wide, Malta isolated carbonate
119 platform (MICP) which aggraded >6 km of Jurassic to Oligocene carbonates over Permo-
120 Triassic continental siliciclastics and carbonates (Fig. 1 d), until it drowned by the end of the
121 Oligocene (Gatt, 2022). The MICP along a passive margin bounded by the Malta and Medina
122 escarpments and was tectonically segmented by NE-SW trending faults that formed a series
123 of ridges and basins described in Gatt (2025). The <1.1 km-thick Cenozoic succession
124 comprises seven formations which are here subdivided into thirteen facies associations
125 named TA to TL (Table 1). The top six Oligo-Miocene formations are exposed in the Maltese
126 Islands.

127 A synthesis of previous research on the Cenozoic tectonics of the Malta Horst, e.g., Gatt
128 (2022), Grasso et al., (1986), Grasso & Pedley (1985), Illies (1981) Martinelli et al., (2019) and
129 Pedley et al., (1976, 1978), allows for the classification of regional deformation into four
130 distinct tectonic phases (A to D) spanning the Late Oligocene to the Pliocene. These tectonic
131 phases have impacted the development of the present phase E contractional deformations
132 deduced from offshore seismic lines, cross sections and well data in the foreland area. The
133 focus of this study is phase E neotectonic contraction in the Malta Horst. Previous studies on
134 neotectonics are limited to small areas of the Malta Horst (e.g., Gardiner et al., 1995; Reuther,
135 1984) whereas this study encompasses a wider area that includes reactivated older faults and
136 new structures observed in seismic imaging along the margins of the Malta Horst which
137 correlate to the hitherto enigmatic dome-shaped topography along the NE coast of Malta
138 Island, described for the first time in the context of anticlinal and synclinal structures. The
139 regional stress field agrees with the plate motion vectors showing ongoing NW compressive
140 deformation in the central Mediterranean and may result in potential geohazards in Malta.

141 The foreland deformations since the Miocene are conceptualised within the context of the
142 temporal change in the rate of migration by the Calabrian Arc with respect to the converging
143 African plate which is key to understanding when contraction or extension prevailed in the
144 central Mediterranean. The objective of this study is to: (1) review the chronology of
145 extensional and contractional phases in the MICP foreland, (2) describe the reactivation of
146 old normal faults by transcurrent movement and the anticlinal and synclinal structures in

147 Malta, (3) assess the role of evaporites in folding and basin inversion tectonics and, (4) discuss
148 the relationship of the Hyblean-Malta Plateau foreland within the geodynamics of the Central
149 Mediterranean.

150

151 **2 Geological Setting**

152 The MICP developed since the Mesozoic on the north African passive margin (Jongsma et al.,
153 1985) (Fig. 1 a) along an abortive rift bounded by the Medina Escarpment (Gatt, 2025) in
154 conjunction with the rifting of the Ionian oceanic crust (Speranza et al., 2012; Tugend et al.,
155 2019). The deep wells confirm >6 km of mostly carbonates in the MICP succession,
156 interbedded by four extensive evaporite beds and two <200 m thick shale beds (lower Jurassic
157 and top Triassic) of continental provenance at the base (Gatt, 2025) related to formations
158 encountered in North Africa (Fig. 1 d). The youngest two evaporite beds were deposited along
159 the Eocene-Oligocene boundary (E1 evaporite bed) and during the Messinian (E0 evaporite
160 bed). The depositional style, absence of siliciclastic deposits and positive bathymetry over
161 surrounding pelagic sediments identify the Maltese carbonates as an isolated carbonate
162 platform (Gatt, 2012; Rusciadelli & Shiner, 2018; Gatt, 2022) comparable to ancient
163 buildups identified in seismic (Burgess, et al., 2013). Jurassic to Cretaceous passive margin
164 extension produced steep faulted margins along the MICP with a throw of 0.5 to >1 km along
165 the NNW trending Malta Escarpment on the east and along the Medina Escarpment in the SE
166 (Finetti, 1982; Jongsma et al., 1985; Tugend et al., 2019; Gatt, 2025). Well data (Fig. 2 a)
167 confirms that the >2 km thick Naxxar Formation (Cretaceous) consists of shallow marine
168 carbonates with gypsum/anhydrite beds (E2 evaporite bed) (Dart et al., 1993; Gatt, 2022).

169 The switch from the Mesozoic passive margin to continental convergence of Africa with
170 respect to Eurasia in the Late Cretaceous (Dewey et al., 1989; Ricou, 1994; Rosenbaum et al.,
171 2002) produced a regional compressive event over northern Africa (Guiraud & Bosworth,
172 1999; Roure et al., 2012) that is equivalent to the Santonian to Paleocene, H-1 depositional
173 hiatus over the MICP (Gatt, 2022) (Fig. 2 c). The compression produced the inversion of the
174 Mesozoic basin along the footwall block (Comino Ridge) described in Gatt (2025). The Comino
175 Ridge and the adjacent inverted basin form the culmination of the West Malta Palaeohigh
176 (WMP) that underlies an area extending from Gozo to the North Malta Graben (Fig. 1 d).
177 Pelagic carbonates of the Lower Globigerina Member (Miocene) thin to <30 m over the WMP
178 (Fig. 3 b) whereas the Middle Globigerina (TG) is entirely missing over eastern Gozo (Pedley
179 et al., 1976).

180 During the early Cenozoic, narrow mobile arcs began to migrate and consume by subduction
181 large parts of the Neotethyan oceanic crust (Faccenna et al., 2004; Malinverno & Ryan,
182 1986; van Hinsbergen et al., 2020). The Calabrian Arc reached the Central Mediterranean
183 by the Neogene (Ciarcia & Vitale, 2024; Jolivet & Faccenna, 2000) producing the
184 accretion of the Sicilian-Maghrebian Thrust belt (Speranza et al., 2018) that began to override

185 the Pelagian sector of the north African plate (van Dijk & Scheepers, 1995). The Malta
186 Group (Cenozoic) sediments (Table 1) reflect the interplay between tectonics and global
187 eustasy based on the sea level curve of Miller et al. (2020) (Fig. 2 d). The late Eocene is marked
188 by the E1 gypsum bed that thickens towards the NW where its dissolution resulted in 300 m-
189 wide sinkholes along the coast of western Gozo (Gatt, 2019) and large caverns encountered
190 at about 600 m depth in the onshore Naxxar deep well. Based on published studies, e.g., Gatt
191 (2022), Grasso et al., (1986), Grasso & Pedley (1985) Illies (1981) Martinelli et al., (2019)
192 Pedley et al., (1976, 1978), the Cenozoic tectonics of the Malta Horst is here categorised into
193 five tectonic phases (A to E in figure 2 d) with the present neotectonic phase E being the
194 subject of this study:

195 **2.1 Phase A (Chattian to Aquitanian)**

196 NW-SE extension during the deposition of the Chattian drowning succession (facies
197 associations TD and TE) of the Lower Coralline Limestone Formation produced the Naxxar
198 Fault which is a 13 km-long normal fault along the WMP footwall block (Fig. 3 a, b) that bounds
199 the Naxxar Basin (Gatt, 2022, 2025) imaged in seismic line 1 as a <7 km-wide depression (Fig.
200 3 a) partly filled with prograding clinoform bedding of facies association TD. Neptunian dykes
201 developed around the margins of the depocentre that were later filled with phosphorite
202 conglomerate (Gatt, 2005) when the MICP drowned by the late Chattian (Gatt et al., 2009).
203 The underfilled Naxxar Basin was later filled with pelagic carbonates of the Lower Globigerina
204 Member (TF) that thicken along the hangingwall from >60 m over Malta Island (locality F in
205 figure 4 a) to 400 m in the offshore depocentre imaged in seismic as post-kinematic horizontal
206 reflectors that unconformably onlap the Oligocene sediments. Although the Naxxar Fault is
207 blind in Malta, locality D close to the fault tip shows the erosive surface along the margin of
208 the footwall block and the overlying transgressive wedge (Fig. 6 h).

209 Nested in the SE margin of the Naxxar Basin is the 5 km wide, Valletta Basin which was first
210 described by Pedley et al. (1976) as an area with a thick succession of Lower Globigerina
211 Limestone which is an important source of building stone in Malta (Gatt, 2006). The Valletta
212 Basin developed as a half graben during the Aquitanian after the MICP drowned at the end of
213 phase A. It is bounded by the Valletta Fault in the west along the Sliema footwall block (locality
214 G). Borehole data confirms that the Valletta Basin is filled with >100 m of pelagic sediments
215 (locality H in figure 4 a) of the Lower Member of the Globigerina Limestone Formation (TF)
216 that thin to <30 m along the upper slope of the roll over anticline forming the East Malta
217 Palaeohigh (EMP). Figure 3 d is a palinspastic reconstruction of the Naxxar and Valletta basins
218 filled with Aquitanian to Burdigalian pelagic sediments. Synthetic faults to the Valletta Fault
219 are exposed along the Valletta peninsula close to locality H (Fig. 6 i) whereas the slope of the
220 hanging block in Birgu is filled with pelagic sediments dipping 10° towards the basin
221 depocentre.

222

223 2.2 Phase B (Burdigalian)

224 Late early Miocene, WNW-ESE extension during the Aquitanian lasted till the Burdigalian and
225 is associated with the growth of small normal faults and basins (Martinelli et al., 2019) filled
226 with pelagic sediments of the Middle Member of the Globigerina Limestone (TG) capped by
227 phosphatic conglomerate filling Neptunian dykes (Dart et al., 1993). The most prominent
228 feature is the Marsaxlokk Basin seen in seismic imaging (Fig. 4 a) which began to develop in
229 the late Aquitanian and peaked in the Burdigalian in SE Malta. The basin shows a thickening
230 of the Middle Globigerina sediments to <100 m, dipping SE, presently preserved as an outlier
231 around Delimara peninsula (Fig. 6 k) (Baldassini & Di Stefano, 2017).

232 2.3 Phase C (Tortonian)

233 The Tortonian compressive event coincides with the H-3 depositional hiatus that terminates
234 the deposition of pelagic marls of the Blue Clay Formation (TI) marking the end of the
235 Serravallian (Hilgen et al., 2009). The regional NW compression produced inversion of older
236 basins in the Ionian Abyssal plain during the Tortonian (Gallais et al., 2011) and significant
237 uplift of the MICP. Bialik et al. (2021) speculate a major uplift of >500 m that permitted the
238 return of shallow marine carbonate sedimentation (TJ and TK) in the Maltese Islands.
239 However, the geodynamics of this phase remain uncertain in the MICP.

240 2.4 Phase D (Messinian to Pliocene)

241 The approaching Calabrian arc produced foreland extension in the Sicily Channel due to slab-
242 pull affect (Argnani, 1990). Most authors also consider the Pantelleria Rift to have begun to
243 develop in the Late Miocene to Early Pliocene (Argnani, 1990; Civile et al., 2021; Dart et al.,
244 1993). In the Maltese Islands, the N-S extension produced two sets of NE and NW trending
245 faults (Fig. 3 c) that control most of the present topography and surrounding bathymetry
246 (Vossmerbäumer, 1972; Illies, 1981; Dart et al., 1993; Bonson et al., 2007):

247 (1) A set of NE-SW trending faults with a throw of <200 m associated with high extensional
248 strain (Putz-Perrier & Sanderson, 2010) that produced the North Gozo Graben in
249 offshore NW Gozo and the North Malta Graben (Fig. 1 b). The latter comprises a series
250 of parallel horsts and grabens, bounded by the South Gozo Fault and the Great Fault
251 that bisects the entire island of Malta (Fig. 3 c).

252 (2) The second set of faults consists of NW-SE trending, conjugate normal faults that form
253 the margins of the Malta Horst: (i) the Sikka Fault along the NE margin with a vertical
254 offset of <100 m (Fig. 3 c) and, (ii) along the SW margin is the Maghlaq fault system
255 (Bonson et al., 2007; Dart et al., 1993) where SW-NE extension produced downthrown
256 blocks that are presently mostly submerged (Fig. 1 c), here sub-divided by five main
257 faults: the inner M1 fault (displacement >200 m) that reaches southern Malta, to the
258 outer M5 fault that is parallel to the Malta Graben Fault (Fig. 3 e), with an overall
259 vertical offset of >1 km. The M4 and M5 faults interact along a NW-dipping relay ramp

260 observed in seismic line 3 (Fig. 4 b) which was later filled by a thick wedge of post
261 kinematic Plio-Quaternary sediments.

262 Footwall upwarping of the Malta Horst along the Maghlaq Fault resulted in the Plio-
263 Quaternary emergence of the Maltese Islands (Illies, 1981) where Pliocene sediments are
264 absent (Gatt, 2007). At the end of phase D, the Messinian drawdown of sea-level resulted in
265 thick evaporite succession in Mediterranean basins (Hsu et al., 1973) and exposed the Malta
266 area to subaerial conditions during the H-4 depositional hiatus which persists in the Maltese
267 Islands as the H-5 depositional hiatus (fig. 2 f).

268

269 **3 Data and methods**

270 The stratigraphy is reconstructed using nine measured sections in localities A to I (Fig. 6 g), 18
271 localities logged by Gatt (2022), boreholes in the Maltese Islands from the Minerals
272 Assessment Report (1996) and water borehole data from Pedley et al. (1976). Limestone
273 texture is based on Dunham (1962) and Embry & Klovan (1971) classifications. Data from
274 deep wells is from the onshore Naxxar-2 (NAX), Zabbar (ZAB) and Madonna taz-Zejt (MTZ)
275 wells and the offshore Gozo (GOZ) and Aqualta (AQU) wells (locations in figure 1 a and b) that
276 have penetrated Cenozoic to Cretaceous sediments. The Paleogene biostratigraphy of the
277 NAX and ZAB wells is re-interpreted by (Gatt, 2012) in the context of more recent biozonation
278 scheme based on benthic foraminiferans by Cahuzac and Poignant (1997) and Serra-Kiel et
279 al., (1998) which is used to date the sediments.

280

281 Six seismic reflection lines are used to interpret the structures affecting the MICP. Seismic line
282 1 lies just outside the Malta Horst and is from a survey carried out in 1980 for the Government
283 of Malta, whereas seismic lines 2, 3, 4 and 5 (Fig. 1 b) are part of a 2-D seismic grid produced
284 by TGS-NOPEC Geophysical Company in 2000-2001 which consist of the Malta Sicily Channel
285 (MSC01) and the Malta Medina Bank (MB01) datasets. The main seismic reflectors and the
286 seismic velocity to depth conversion is based on data from the AQU well (Fig. 2 b) which is
287 correlated to rock outcrops and deep wells in Malta. The methodology used in this study is
288 based on the correlation of the geometry of structures seen in seismic line 2 with the
289 topography of the NE coast of Malta. Present in situ strain measurements of near surface
290 stress in Malta are from Grasso et al. (1986) using the doorstopper method.

291

292

293

294

295 **4 Results**

296 **4.1 Main seismic discontinuities**

297 The data collected from wells and outcrop localities A to I are used to interpret offshore
298 seismic lines and construct geological cross sections on land. Six strong reflectors, M, B-C, O,
299 C, E and K-reflectors described by Gatt (2025) are identified in seismic lines (Fig. 2 b and Table
300 1) which correlate to lithological boundaries that mark depositional hiatuses H-1 to H-4, of
301 which the H-3, H-4 and H-5 are observed in the Maltese Islands (Fig. 2 c). The six reflectors
302 within the Malta Group (Cenozoic) are bounded by the M-reflector at the top and the K-
303 reflector at the base with the intermittent E-reflector having an important role:

304 M-reflector: marks the Messinian draw down of sea-level that produced subaerial conditions
305 over large parts of the Mediterranean (Hsu et al., 1973; Krijgsman et al., 1999; Roveri et al.,
306 2014), corresponding to the H-4 depositional hiatus in the MICP that terminates
307 sedimentation in the Upper Coralline Limestone Formation (TJ and TK) which consists of
308 shallow marine carbonates (Pedley, 1978). The M-reflector is capped by Plio-Quaternary
309 sediments along the margins and outside the Malta Horst.

310 O-reflector: corresponds to the termination of shallow marine sedimentation when the MICP
311 drowned and was draped by pelagic sediments of Globigerina Limestone Formation (facies
312 association TF).

313 C-reflector: marks the abrupt change from interior, fine-grained carbonate platform
314 sediments (facies association TC) to coarse-grained drowning succession (TD).

315 E-reflector: corresponds to the E1 gypsum bed, an evaporite bed deposited in a sabkha type
316 of environment capping the Ypresian shallow marine carbonates of the Zabbar Formation
317 consisting of *Alveolina* packstones (Gatt, 2022). The age of the gypsum bed may range from
318 middle to late Eocene and was deposited during the circa 15 Ma long, H-2 depositional hiatus.

319 K-reflector: The H-1 depositional hiatus marks a 27 Ma-long biostratigraphy gap that
320 terminates Cretaceous carbonate sedimentation of the Naxxar Group (Gatt, 2022). The
321 horizon is characterised by cavernous porosity, breccia and a thin lignite bed encountered in
322 NAX and ZAB wells which suggests a karstic surface along the exposed MICP which was
323 uplifted by compression that resulted in anticlinal structures (Gatt, 2025). Several thrusts are
324 observed in seismic along the topmost Naxxar Formation (Cretaceous) resulting from
325 compression during phase C.

326 Several structures occur in different parts of the Malta Horst which is here sub-divided into
327 five areas (Fig. 4) based on the type of structures. This study focuses on deformation along
328 the NE margin (Area 1) of the Malta Horst that extends from the Sikka Fault to a series of
329 domes and ridges along a <10 km wide belt along the NE coast of Malta island:

330

331 **4.2 Area 1**

332 Tectonic Phase E resulted in differential deformation across the various segments of the Malta
333 Horst.

334 Faults:

335 The NE margin of Area 1 is bounded by the Sikka Fault and the Hurd Bank Fault, south of
336 Malta. The latter is a right-lateral strike-slip fault seismically imaged by line 5 (Fig. 4 c) showing
337 a negative flower structure. The NW trending south Sikka Fault developed as a normal fault
338 during phase D (Line 6) but is now reactivated as a right-lateral strike-slip fault (Fig. 3 e).

339 Contractional deformation:

340 Seismic line 2 shows a series of thrust faults dipping $<40^\circ$ with overlying anticlines (Fig. 4 a).
341 The position of these anticlines in seismic imagery correlates with <4 km wide topographic
342 highs observed along the NE coast of Malta where the Lower Coralline Limestone Formation
343 is >50 m above sea level (Fig. 5 a). Felix (1973) and Pedley et al. (1976) describe these hitherto
344 enigmatic folds in Malta as the 'Naxxar Dome' and Zabbar culmination where the Lower
345 Coralline Limestone Formation in these areas reaches 120 m and 50 m asl, respectively.
346 However, no explanation is given for their formation, although they are known to be
347 associated with positive gravity anomalies (Harrison, 1954) implying that older and denser
348 rock is closer to the surface. These gravity anomalies attracted the drilling of the first onshore
349 hydrocarbon dry wells in namely, the NAX and ZAB dry wells in the 1950s.

350 Cross-sections in figure 6 are based on well data and measured outcrops in Malta within Area
351 1 and show a series of anticlinal and synclinal structures along the NE coast of Malta overlying
352 six thrust faults labelled 1 to 6 in Figure 6 b where the Naxxar Dome and the Zabbar
353 culmination are interpreted as the Naxxar and Zabbar anticlines. The emergent thrust system
354 is extensively eroded in SE Malta where the topography created by anticlines is mostly
355 obliterated but more preserved towards the NW. The thrusting resulted in basin inversion
356 and uplift so that the top of the Lower Coralline Limestone Formation is presently 120 m asl
357 (thrust 4 in Fig. 5 a). A succession of four main anticlines separated by synclines that extend
358 from the SE to the NW in Area 1 are observed:

359 4.2.1 Marsascala Anticline and Marsaxlokk Basin

360 A nearly symmetrical anticline (thrust 1) is observed in seismic imagery (Fig 3 b) with its
361 western end emergent on land. Contraction along the Marsascala thrust fault uplifted Oligo-
362 Miocene sediments, exposing the Lower Coralline Limestone Formation along Marsascala
363 Bay. In seismic line 2, the thrust fault soles along the E1 evaporite bed (Fig. 4 a) and Miocene
364 pelagic sediments show some thinning over the anticline which suggests Messinian erosion.

365 The slight bathymetric shallowing over the anticline implies post-Messinian uplift. The NW
366 margin of the Marsaxlokk Basin is partly subaerial along the Delimara peninsula where it
367 forms the dorsal part of the Marsascula Anticline. The exposed Middle and Upper members
368 of the Globigerina Limestone dip towards the SE in the direction of a depression that formed
369 by Burdigalian extension (Fig. 6 b).

370 4.2.2 Zabbar Anticline and San Leonardo Syncline

371 In seismic imaging (Fig. 4 a), the Zabbar Anticline forms the frontal part of the imbricate thrust
372 system involving Oligo-Miocene sediments that extends to the Marsascula Anticline. Thrust
373 faults 2 and 3 (Fig. 6 b) sole along the E-reflector gypsum bed decollement with the overlying
374 synkinematic Miocene pelagic sediments mostly preserved. On land, erosion has exhumed
375 facies association TE along the emergent Zabbar Anticline and the underlying Migra Ferha
376 Member (TD2) at Tar-Ramel along the anticline hinge zone (Fig. 6 c). The backlimb of the
377 anticline is fractured by extension which produced several <50 m wide grabens passing
378 laterally to the syncline farther east, here named the San Leonardo depression. This
379 palaeobathymetric low between the Zabbar and Marsascula anticlines accumulated the
380 shallow marine carbonates of the San Leonardo Formation deposited at depths of 10 to 30 m
381 (TL) during the Calabrian sea level highstand (Pedley, 2011). The relatively resistant San
382 Leonardo carbonates unconformably cap and preserve the much weaker underlying Middle
383 Globigerina Limestone.

384 4.2.3 Valletta Anticline

385 The Valletta Fault (thrust 4) and its 1 km apart, antithetic Grand Harbour Fault were
386 reactivated as reverse faults during phase E (Fig. 6 b). Both faults are presently submerged
387 but can be inferred by the geometry of the sediments. Contraction resulted in basin inversion
388 that raised the Valletta Basin depocentre to 50 asl., which is 20 m higher than the adjacent,
389 pre-inversion footwall block in Sliema (Fig. 6 b). The nearly symmetrical, doubly plunging, NE-
390 SW trending Valletta Anticline presently forms the backbone of the Valletta peninsula
391 composed of the Lower Globigerina Limestone (TF). East of the Grand Harbour Fault, the Birgu
392 Depression preserves the basinward dipping pelagic (TF) sediments exposed at Birgu along
393 the undeformed upper hangingwall slope of the Valletta Basin.

394 4.2.4 Naxxar Anticline and Sliema-Hamrun Syncline

395 The cross sections of the Naxxar Anticline (Figs. 6 a, b, and f) show a non-cylindrical anticline
396 that doubly plunges, inland to the SW and to the NE (Fig. 5 b) where it forms a submerged
397 shoal along the margin of the Malta Horst. The anticline attains a maximum height of 145 m
398 and its core along the eroded culmination of the pericline is exposed at locality C (Mosta
399 quarry) where facies association TC is exhumed (Fig. 6 b and e). The Naxxar Anticline formed
400 along a reactivated onshore segment of the Naxxar Fault that produce basin inversion of part
401 of the Naxxar Basin. Outside the Malta Horst, the Naxxar Basin depocentre remains

402 undeformed as seen in seismic line 1 (Fig. 3 a). The angle of the upper part of the Naxxar listric
403 fault is too steep for reactivation as a reverse fault so that a footwall shortcut (thrust 6)
404 developed at a lower angle which surfaces about 200 m farther west from the main fault. The
405 thrust fault is imaged in seismic line 2 and exhumed the Lower Coralline Limestone Formation
406 on land and offshore (Fig. 5 a, b, 6 b and e).

407 The frontal part of Naxxar Anticline comprises the 1.5 km-wide, Wied Faham Overthrust (Fig.
408 7 a and b) that migrated horizontally by >100 m along a low angle (~25°) reverse fault across
409 part of the older Great Fault (phase D). The deformed floor thrust sediments dip by 15° ESE
410 (Fig. 7 b i) and the roof thrust dips at <10° (Fig. 7 b ii). The Wied Faham Overthrust developed
411 into an overturned fold as it migrated westward along a low angle axial plane verging NW
412 over the ductile Blue Clay Formation (Fig. 7 c) which was smeared along the floor thrust and
413 acted as a decollement surface. The mass of the overthrust downflexed the hangingwall
414 margin of the older Great Fault, preserving an outlier of younger rock (TG and TH) along its
415 flank (Fig. 7 b).

416 The dorsal part of the Naxxar Anticline hosts the Sliema-Hamrun Syncline (Fig. 5 b) that doubly
417 plunges to the SW towards Hamrun Basin and to the NE towards Sliema Syncline, separated
418 by the Pieta Anticline (Fig. 6 d and f). The Sliema end consists mostly of Lower Globigerina
419 Limestone (TF) with a small outlier of Middle Globigerina (TG) preserved in the hangingwall
420 of the Tigne Fault (Gatt, 2005) at locality G (Fig. 5 b). A larger outlier of the Middle Globigerina
421 Member is preserved along the Hamrun end of the syncline over central Malta (Fig. 6 a, d,
422 and f). The Sliema and Hamrun synclines are separated by the Pieta Anticline which is a <2 km
423 long, imbricated in front of the larger Valletta Anticline. The Pieta Anticline interferes with
424 the Sliema-Hamrun Syncline and exhumes the Lower Globigerina along its centre, preserving
425 the Middle Globigerina along its flanks (Fig. 6 d).

426 **4.3 Area 2**

427 The wedge-shaped area extends from the Great Fault on the northwest to the eastern tip of
428 the Maghlaq Fault (M1) on the south (Fig. 3 e).

429 Faults: Older faults formed during tectonic phase D are preserved mostly consisting of
430 Miocene, NE trending faults.

431 Horizontal deformation:

432 This western part of Malta exhibits uparching of the Lower Coralline Limestone Formation
433 which reaches a thickness of 120 m along the cliffed coast of Malta (Fig. 5 a) during tectonic
434 phase E contraction. The deformation produced a NE trending anticline exposed along the
435 cliffed coast of Malta. The NW limb dips by 2° towards the NW with a lower angle dip along
436 the SE limb. Synclines oblique to the Maghlaq Fault (M1) on land preserve a Middle
437 Globigerina outlier along the Mqabba Basin (Fig. 5 a and 6 h). Most of the Malta Group

438 sediments (TD to TK) are preserved along the western part of Area 2 (Fig. 6 k), in contrast to
439 Area 1 where sediments younger than the Aquitanian are mostly eroded.

440

441 **4.4 Area 3**

442 Area 3 consists of a 13 km wide offshore belt along the SW-facing margin of the Malta Horst
443 that hosts the offshore part of the Maghlaq Fault system. The area is crossed by seismic line
444 3 (Fig. 4 b) parallel to the outer Maghlaq fault system (M4 and M5).

445 Faults:

446 The inner part of the WNW trending Maghlaq fault system (M1) is exposed in Malta as a
447 normal fault showing minor sinistral slip component (Bonson et al., 2007). An earthquake
448 swarm in 2015 (Bozionelos et al., 2017) between the M1 and M2 faults and older earthquakes
449 around M3 fault suggest that they are active (Fig. 3 e). The southern margin of Area 3 is
450 bounded by the NW trending outer Maghlaq faults (M4 and M5) which are parallel to the
451 Malta Graben master fault. The M5 fault of the Maghlaq fault system developed as normal
452 faults during phase D and is presently reactivated as left-lateral strike slip faults (phase E).

453 Horizontal deformation:

454 Seismic line 3 along the SE margin of Area 3 shows uplifted Cretaceous sediments deformed
455 by compression capped by a relatively thin Zabbar Formation (Eocene) overlain by a series of
456 listric faults through the Oligo-Miocene succession showing minor thrusts verging NW. The
457 thrusts do not extend to Malta island, except for the here-named Filfla Fault and overlying
458 anticline (Fig. 4 b) which resulted in subaerial exposure of only part of the hangingwall block
459 of the M1 Maghlaq Fault in Malta island and the tiny Filfla island (Fig. 3 e). The thrusts
460 observed in seismic imaging (line 3 in figure 4 b) sole along the E1 gypsum bed (E-reflector).
461 Farther west, sediments dip NW along the relay ramp between the outer Maghlaq faults (M4
462 and M5) which is partly filled with Plio-Quaternary sediments. Seismic line 5 shows anticlines
463 on both sides of the M1 and M2 Maghlaq faults in offshore south Malta. These features
464 suggest compression orthogonal to the inner Maghlaq fault system (Fig. 3 e).

465 **4.5 Area 4**

466 Area 4 entirely overlies the West Malta Palaeohigh (WMP), which constitutes the footwall
467 block of the Naxxar Basin (Fig. 1 d). Phase E deformation in this region is characterized
468 primarily by strike-slip kinematics and associated minor folding, largely driven by the
469 reactivation of existing structures. The South Gozo Fault, originally characterized by 100 m of
470 vertical displacement during the Late Miocene (phase D), now exhibits a dextral strike-slip
471 overprint (Fig. 5 d). The transcurrent movement created 250 m-wide feather structures by
472 extension along the eastern part of the fault (Reuther, 1984) whereas compression in the

473 western part resulted in the development of an anticline exposed along the coast. Parallel to
474 this W-E trending fault are the South Comino strike-slip fault (Fig. 5 a) and the dextral strike-
475 slip Bugibba Fault exposed along the coast where fault breccia from the underlying Lower
476 Coralline Limestone Formation is exhumed along the fault with Riedel shears developing in
477 the surrounding Lower Globigerina Limestone (TE) (Fig. 6 j). En echelon strike-slip faults also
478 formed around the southern part of the Mellieha Ridge (Fig. 5 c).

479 The NE-trending Miocene normal faults within the North Malta Graben show evidence of
480 reactivation and minor upthrusting (Reuther and Eisbacher, 1985) whereas the West Malta
481 Fault (Figs. 3 e) aligned with the regional compression field, functions as a strike-slip structure
482 exhibiting transpression, which has resulted in the formation of a positive flower structure
483 (Fig. 4 d).

484

485 **5. Discussion**

486 During Phase E, NW-directed contraction reactivated pre-existing Oligo-Miocene normal
487 faults through two distinct structural mechanisms:

488 1. Strike-Slip Reactivation: Normal faults running parallel to the NW–SE trending margins
489 of the Malta Horst (specifically the Sikka and Maghlaq faults) are reactivated as strike-
490 slip faults trending sub-parallel ($<30^\circ$) to the NW-directed compressional regime (σ_1).
491 The neotectonic structures mapped in figure 8 a, show several focal mechanisms of
492 earthquakes associated with this strike-slip type of movement (Maiorana et al., 2023).
493 These structures align to synthetic Riedel shears shown in figure 8 b which typically
494 constitute the first surface features to develop (Tchalenko, 1970).

495 2. Thrust Reactivation: Normal faults trending oblique (NE–SW) or orthogonal to the
496 horst margins (such as the Naxxar and Valletta faults) were reactivated as reverse
497 faults. These developed into NW-verging thrusts characterized by overlying anticlines.

498

499 **5.2 Regional tectonics**

500 At the regional level, phase E contraction is consistent with the occurrence of Quaternary NW
501 deformation in Tunisia (Bouaziz et al., 2002), the development of anticlines in the Linosa
502 Graben and northern Malta Graben (Maiorana et al., 2023; Sulli et al., 2021; Civile et al.,
503 2021) and drives a right-lateral motion component of $1.7 \pm 0.8 \text{ mm yr}^{-1}$ along NW-SE striking
504 fault systems between North Africa and Lampedusa Island (Serpelloni et al., 2007).

505 Phase E occurs at a time of slowing down or stopping of the rollback of the Calabrian arc as
506 shown by GPS data (Serpelloni et al., 2007), accompanied by the locking of the subduction

507 fault in the Ionian sector (Gutscher et al., 2006). The end of rollback terminated foreland
508 extension by slab-pull affect (phase D) and subjected the Pelagian foreland to the ongoing
509 NW compression by Africa with respect to Eurasia at a rate of ~ 0.5 mm/yr (Nocquet, 2012;
510 Serpelloni et al., 2022) and NW-SE shortening (Palano et al., 2020) as confirmed by GPS
511 stations in southern Sicily, Malta and the Sicily Channel that match the African plate motion
512 (Goes et al., 2004) and the NW horizontal stress and strain in the central Mediterranean
513 region (Ragg et al., 1999; Zoback, 1992).

514 The NW-directed compression of the rigid HMP crust induced regional strain, facilitating the
515 displacement of structural blocks such as the Malta Horst. The dextral strike-slip movement
516 along the Sikka Fault suggests the anticlockwise rotation of the block north of the Malta Horst
517 and the extrusion of the Malta Horst block towards the NW, into the North Gozo Graben and
518 Area 5 where several contractional anticlines have developed (Gardiner et al., 1995) (Fig. 8
519 a). However, the shearing and contraction of Oligo-Miocene sediments observed in Areas 1,
520 3 and 5 (outside the WMP) are thin-skinned features (Fig. 1 d), associated with shallow depth
521 (< 5 km) earthquakes whereas many earthquakes in the Malta Horst occur at a depth of about
522 10 km (INGV, 2025), which is close to the interface of the MICP sediments with the African
523 granitic basement (Fig. 1 d) (Gatt, 2025). At this depth, deformation is dominated by the West-
524 East trending Principal Displacement Zone (PDZ).

525 The strain ellipse in figure 8 b shows the PDZ that developed in response to Northwest-
526 directed stress (σ_1) within the North African craton. The PDZ developed by W-E transcurrent
527 movement since < 5 Ma that produced the dextral strike-slip movement of the Medina
528 Wrench which forms a 300 km long belt of transcurrent deformation along the southern
529 boundary of the HMP microplate which is moving eastward with respect to Africa (Jongsma
530 et al., 1987). Some authors suggest that the deep grabens within the Pantelleria Rift
531 developed as pull-apart basins along this dextral shear zone (Boccaletti, 1987; Jongsma et
532 al., 1987; Reuther & Eisbacher, 1985) in response to transcurrent movement along the
533 Medina Wrench (Fig. 8 c). The W-E strain is manifest in the Malta Horst in two areas:

- 534 a. The WNW trending eastern part of the Malta Graben Fault that is subparallel to the
535 Medina Wrench,
- 536 b. Along the W-E transcurrent faults in Area 4 which are aligned with the Medina Wrench
537 (Fig. 8 a). This alignment likely stems from the structural high of the Mesozoic WMP which
538 is close to the surface (Fig. 1 d). Consequently, the underlying W-E thick-skinned
539 deformation is expressed at a more advanced stage of surface emergence.

540 The W-E strain along these two zones frames a 50 km-wide pull-apart basin encompassing
541 the Maltese Islands, bounded on the west by the Malta Graben/Maghlaq faults and on the
542 east by the Sikka/Hurd Bank first-order strike-slip. The fault geometry implies an active, W-E
543 dextral transcurrent movement and diverging NE-SW strain-stress regime (σ_3), albeit with a
544 low deformation rate (Fig. 8 d).

545 **5.3 Geometric analysis: NW-SE strike-slip faults**

546 The right-stepping Sikka strike-slip faults produced a series of <5 km-wide, W-E trending
547 extensional oversteps that form small pull-apart basins along the margins of the Malta Horst
548 (Fig. 8 d). One of these basins is along the right-stepping South Sikka fault and Hurd Bank
549 Fault. Extension produced the transtensional strike-slip Hurd Bank fault with a negative flower
550 structure imaged in seismic line 5 (Fig. 4 c) along its NW tip. At least two other basins are
551 inferred from bathymetry in the hangingwall block of outer Maghlaq fault (M5). In contrast,
552 transpression is implied along the South Sikka Fault from the *in situ* stress measurements (Fig.
553 5 b). The transpression resulted in drag along the transcurrent fault which produced the
554 folding observed along the NE coast of Malta (Area 1).

555 It is suggested that the central part of the Horst Malta is under minor compression along a
556 crescent-shaped zone that extends from the NNW trending West Malta Fault (dextral strike-
557 slip fault imaged along seismic line 4 in Figure 4 d) to the east part of the Maghlaq Fault
558 imaged in seismic line 5. Both faults show positive flower structures in seismic, implying
559 transpression which may be accommodating extension along the conjugate margins of the
560 Malta Horst.

561

562 **5.4 NE-SW faults and folds and the E1 evaporite bed**

563 Pre-Cenozoic contractional deformation of Mesozoic MICP sediments (Gatt, 2025) indicates
564 a more rigid rheology compared to the younger Oligo-Miocene sequence. Because of its rigid
565 rheology, the WMP acts as a backstop for Oligo-Miocene deformations (Fig. 1 d). In regions
566 of greater Oligo-Miocene thickness (Areas 1, 3, and 5), the resulting differential horizontal
567 strain between the rigid Mesozoic basement and cover is resolved by strain along the E1
568 décollement.

569 The E1 gypsum bed is overlain by 20 m of argillaceous limestone, penetrated by the NAX and
570 ZAB wells. These low shear strength beds are characterised by 50 m of breccia with large,
571 cavernous porosity (Fig. 2 a). The fracturing and caverns suggest dissolution of the gypsum
572 bed observed in the NAX and ZAB wells (Fig. 2 a) and extensive shearing along the decollement
573 over the which the Oligo-Miocene succession translated. The regional NW compression
574 resulted in reactivation of parts of the older NE-SW trending normal faults (phase A) into
575 thrusts that sole along the E1 gypsum bed at the Eocene-Oligocene boundary (seismic line 2).
576 The thrusts are overlain by NW-verging folds that extend to <10 km along the NE margin of
577 the Malta Horst (Area 1) which are exposed along the NE coast of Malta as a series of non-
578 cylindrical and doubly plunging folds. These en echelon folds developed at a 45° angle to the
579 Sikka strike-slip faults (Fig. 5 a) in the direction of shear as suggested by Sylvester (1988). The
580 anticlines form an imbricate thrust system around the Marsascula Anticline with more
581 isolated and increasingly asymmetrical folds farther northwest. The latter folds are associated
582 with basement structures of the Naxxar and Valletta normal faults (tectonic phase A) that

583 seeded thin-skinned folds and basin inversion. The well-preserved, dome-shaped Naxxar
584 Anticline involved the reactivation of only a small section of the Naxxar Fault, which suggests
585 that the remainder of this fault has a dip angle too steep ($>60^\circ$) for reverse fault reactivation
586 (Sibson, 1995). Nevertheless, the reactivated section developed a shortcut fault (fault 6 in
587 figures 4 a and 6 b) in response to the steep angle of the Naxxar Fault.

588 In Area 1 and the eastern half of Area 2, only the Lower Globigerina Limestone and Lower
589 Coralline Limestone formations are preserved. The Upper Coralline Limestone and Blue Clay
590 formations were entirely removed by extensive erosion during the Phase E thrust uplift.
591 However, outliers of Middle and Upper Globigerina members (TG and TH) and San Leonardo
592 Formation (TL) are preserved in the synclines (Fig. 6 k). In eastern Malta, the deep erosion of
593 the Marsascala and Zabbar anticlines indicates they are older than the Naxxar Anticline to the
594 west. This pattern suggests that thrusting moved from east to west over time. While thrust
595 fault tips remain buried within the older anticlines of eastern Malta, they are exhumed along
596 the Valletta and Grand Harbour faults. In these locations, Messinian palaeorivers
597 preferentially eroded the sheared rock during glacial sea-level drawdowns, carving valleys
598 that were subsequently submerged during Pliocene flooding (Fig. 5 b).

599 The effect of transcurrent movement dissipates farther away from the margins of the Malta
600 Horst, so that folds observed along the margins (Areas 1 and 3) do not extend to the central
601 part of the Malta Horst. The main deformation in the middle of the horst (Area 2) are synclines
602 related to transpression along the Maghlaq Fault. Thrusting with overlying anticlines is more
603 subtle in Area 3 relative to Area 1 and affects a smaller area.

604

605 **5.5 Dating of regional contraction**

606 The Medina Wrench exhibits deformation since 5 Ma (Jongsma et al., 1985) along with the
607 development of the Pantelleria Rift (Reuther & Eisbacher, 1985) whereas N-S extension
608 (phase D) ended at 1.5 Ma marking the post-rift stage of the graben systems in Malta (Dart et
609 al., 1993). The early stage of phase E (<1.5 Ma) began at this time when W–E transcurrent
610 movement along the Medina Wrench reactivated the NW-trending normal faults of the Malta
611 Horst into strike-slip faults (Fig. 2f). The NW stress and accumulated transcurrent drag along
612 NW-striking faults resulted in tectonic inversion of the existing NE-trending normal faults,
613 which were reactivated as thrusts along the margins of the Malta Horst. However, the precise
614 dating of the late stage of phase E is uncertain mainly because Quaternary sediments are
615 mostly terrestrial and sparsely preserved except in valleys. The exception is the San Leonardo
616 Formation (Calabrian stage) that was deposited in shallow sea (maximum depth of 10–30 m)
617 (Pedley, 2011) but is presently located >50 m asl. Given that the Calabrian stage eustatic
618 highstands reached only a few meters above modern sea level (Miller et al., 2005) the current
619 elevation of the San Leonardo Formation (TL) marine sediments necessitates significant (>60

620 m) post-depositional tectonic uplift. This uplift was likely driven by the underlying San
621 Leonardo thrust which forms part of an imbricate thrust system (thrust fault 2 in figure 6 b).
622 The well-cemented shallow marine sediments (TL) were preserved within a synclinal structure
623 and with subsequent upthrusting, the soft pelagic sediments of the adjacent Zabbbar and
624 Marsascala anticlines were truncated by erosion. Based on the Calabrian age of the San
625 Leonardo beds proposed by Pedley (2011), upthrusting associated with the late stage of
626 phase E began right after the Calabrian stage (<0.7 Ma), which coincides with the end of
627 Calabrian arc rotation (van Dijk & Scheepers, 1995).

628 Northwest verging thrusting continued during the Holocene in the Valletta Anticline and
629 culminates in the Naxxar Anticline. Holocene core data from Marsa (2 km from Valletta
630 Anticline) shows tectonic uplift of about 2 m since 6500 cal. BP (Carroll et al., 2012) which
631 implies uplift related to the Valletta Anticline during the mid-Holocene. Uplift of the Naxxar
632 Anticline at the same time may have contributed to the significant increase in sediment supply
633 in the north flowing palaeoriver of Wied il-Ghasel (Fig. 5 b) recorded by Marriner et al. (2012),
634 which suggests rejuvenated vertical erosion upstream related to anticline uplift.

635 **5.6 Geohazards**

636 Most of the larger earthquakes recorded in Malta have their epicentres in Sicily, the Sicily
637 Channel or Greece (Barbano et al., 2021). This study shows that there are another three
638 potential mechanisms for seismic activity much closer to the Maltese Islands: (1) The present
639 ongoing strike-slip movement along NW trending faults which results in low magnitude (M
640 <4) earthquakes very close to Malta as happened in 2015 (Bozionelos et al., 2017) and April
641 2025 magnitude 3.5 earthquake at depth of 20.8 km near the Sikka Fault (INGV, 2025) (Fig. 3
642 e), (2) the reactivation of <10 km-long sections of older NE-SW trending faults along the
643 margins of the Malta Horst (Areas 1 and 3) and the W-E transcurrent strain in Gozo (Area 4)
644 and along the eastern Malta Graben Fault.

645 No recorded earthquakes are known to be directly related to the thrust faults, although the
646 direction of horizontal compressive stress recorded in situ by Grasso et al. (1986) along the
647 NE coast of Malta (Fig. 5 b, c) is consistent with the NW vergence of anticlines in Area 1. The
648 absence of known seismic activity associated with these thrust faults may be due to one of
649 the following:

- 650 1. Aseismic translation of the thrust planes along the E1 decollement,
- 651 2. The NW horizontal stress becomes stored as elastic energy which is only released when
652 the static friction along the thrust plane is overcome, resulting in a seismic event (Doglioni,
653 2024). The absence of known earthquakes along the thrusts planes means that the
654 recurrence of such a seismic event is longer than the first historical record of earthquakes,
655 which in Malta is 1542 (Galea, 2007). The long recurrence period is related to the steep
656 angle of the thrusts.

657 The second mechanism is more likely as transcurrent movement along the Sikka and Maghlaq
658 faults builds up elastic energy by drag affect along the Malta Horst margins. The deep-seated
659 W-E transcurrent movement in Area 4 is another source of deep earthquakes linked to
660 deformation of the basement (Fig. 1 d). The overall scenario may result in strong earthquake
661 with epicentres very close to Malta in the future.

662

663 **6. Conclusion**

664 The Malta Horst forms the southern part of the Hyblean-Malta Plateau (HMP) which entered
665 a foreland position since the Miocene. It is characterised by:

666 - Alternating phases of extension (phases A, B and D) and contraction (phases C and E). The
667 extensional phases produced successive basins: the Naxxar, Valletta, and Marsaxlokk half
668 grabens (Oligocene-early Miocene) and the North Gozo, North Malta, and Malta grabens (Late
669 Miocene-Pliocene).

670 -The change from an extensional (phase D) to the present contractional (Phase E) regime
671 marks the slowing down of the velocity of the Calabrian arc as it migrated SE towards the
672 north African foreland. The slowdown ended foreland extension in the HMP. The present
673 contraction reflects the resumption of the dominance of ongoing convergence of Africa
674 towards Eurasia since the Late Cretaceous.

675 -The present contractional phase E reactivated the Late Miocene to Pliocene, NW trending
676 normal faults (phase D) parallel to the margins of the Malta Horst by dextral transcurrent
677 movement to accommodate the compression.

678 - The NW compressive event reactivated the NE trending Oligo-Miocene faults into thrusts
679 and inverted half grabens of phase A into a series of NW-verging anticlines and synclines
680 oblique to the margins of the Malta Horst (Areas 1 and 3). The Oligo-Miocene sediments
681 underwent thin-skinned contraction facilitated by late Eocene to early Oligocene evaporite
682 and marly beds acting as a decollement surface.

683 -The underlying Mesozoic basement (West Malta Palaeohigh) acted as a backstop to thin-
684 skinned thrusting. Deformation in Area 4 (WMP) is along W-E strike-slip faults and reflects the
685 regional PDZ from NW compression.

686 -Present compression is pushing the Malta Horst towards the NW into Area 5 where thin-
687 skinned deformation by folding is common.

688 -The compressive structures in Malta are still active, although not associated with historical
689 seismic events which suggests either slow ductile deformation along evaporite décollements
690 or a long recurrence period of seismic events.

691

ACKNOWLEDGEMENTS

692 BP and Total are thanked for providing well data and TGS for the seismic sections. I thank the
693 Editor Prof Juan Soto for his comments on the text and encouragement as well as two other
694 anonymous reviewers. This study is partly based on the author's PhD thesis at the University
695 of Durham, UK.

696

697

698

REFERENCES

- 699 Argnani, A. (1990). The Strait of Sicily rift zone: foreland deformation related to the
700 evolution of a back-arc basin. *Journal of Geodynamics*, 12, 311–331.
- 701 Baldassini, N., & Di Stefano, A. (2017). Stratigraphic features of the Maltese Archipelago: a
702 synthesis. *Natural Hazards*, 86, 203–231. <https://doi.org/10.1007/s11069-016-2334-9>
- 703 Bally, A. W. (1984). Tectogenese et sismique reflexion. *Bulletin de La Société Géologique de*
704 *France*, S7-XXVI(2), 279–285. <https://doi.org/10.2113/gssgfbull.S7-XXVI.2.279>
- 705 Barbano, M. S., Castelli, V., Galea, P., & Pirrotta, C. (2021). Materials for a seismic history of
706 the Maltese Islands. *Quaderni Di Geofisica*, 171, 1–358.
707 <https://doi.org/10.13127/qdg/171>
- 708 Ben-Avraham, Z., Lyakhovsky, V., & Grasso, M. (1995). Simulation of collision zone
709 segmentation in the central Mediterranean. *Tectonophysics*, 243(1–2), 57–68.
710 [https://doi.org/10.1016/0040-1951\(94\)00191-B](https://doi.org/10.1016/0040-1951(94)00191-B)
- 711 Bialik, O. M., Zammit, R., & Micallef, A. (2021). Architecture and sequence stratigraphy of
712 the Upper Coralline Limestone formation, Malta—Implications for Eastern
713 Mediterranean restriction prior to the Messinian Salinity Crisis. *Depositional Record*,
714 7(2), 256–270. <https://doi.org/10.1002/dep2.138>
- 715 Boccaletti, M. (1987). Transtensional tectonics in the Sicily Channel. *Journal of Structural*
716 *Geology*, 9(7).
- 717 Bonini, M., Sani, F., & Antonielli, B. (2012). Basin inversion and contractional reactivation of
718 inherited normal faults: A review based on previous and new experimental models.
719 *Tectonophysics*, 522–523, 55–88. <https://doi.org/10.1016/j.tecto.2011.11.014>
- 720 Bonson, C. G., Childs, C., Walsh, J. J., Schöpfer, M. P. J., & Carboni, V. (2007). Geometric and
721 kinematic controls on the internal structure of a large normal fault in massive
722 limestones: The Maghlaq Fault, Malta. *Journal of Structural Geology*, 29(2), 336–354.
723 <https://doi.org/10.1016/j.jsg.2006.06.016>
- 724 Bouaziz, S., Barrier, E., Soussi, M., Turki, M. M., & Zouari, H. (2002). Tectonic evolution of the
725 northern African margin in Tunisia from paleostress data and sedimentary record.
726 *Tectonophysics*, 357, 227–253.

- 727 Bozionelos, G., Galea, P., D'Amico, S., & Agius, M. (2017). Characteristics of the recent
728 seismic activity on a near-shore fault south of Malta, Central Mediterranean.
729 *Geophysical Research Abstracts EGU, 19*, 2017–17929.
- 730 Cahuzac, B., & Poignant, A. (1997). Essai de biozonation de l'Oligo-Miocene dans les bassins
731 europeen a l'aide des grands foraminiferes neritique. *Bull. Soc. Geol. France, 168*(2),
732 155–169.
- 733 Carroll, F. A., Hunt, C. O., Schembri, P. J., & Bonanno, A. (2012). Holocene climate change,
734 vegetation history and human impact in the Central Mediterranean: Evidence from the
735 Maltese Islands. *Quaternary Science Reviews, 52*, 24–40.
736 <https://doi.org/10.1016/j.quascirev.2012.07.010>
- 737 Ciarcia, S., & Vitale, S. (2024). Orogenic evolution of the northern Calabria–southern
738 Apennines system in the framework of the Alpine chains in the central-western
739 Mediterranean area. *Geological Society of America Bulletin*.
740 <https://doi.org/10.1130/B37474.1>
- 741 Civile, D., Brancolini, G., Lodolo, E., Forlin, E., Accaino, F., Zecchin, M., & Brancatelli, G.
742 (2021). Morphostructural Setting and Tectonic Evolution of the Central Part of the
743 Sicilian Channel (Central Mediterranean). *Lithosphere, 2021*(1), 1–24.
744 <https://doi.org/10.2113/2021/7866771>
- 745 Cogan, J., Rigo, L., Grasso, M., & Lerche, I. (1989). Flexural tectonics of southeastern Sicily.
746 *Journal of Geodynamics, 11*(3), 189–241. [https://doi.org/10.1016/0264-](https://doi.org/10.1016/0264-3707(89)90007-0)
747 [3707\(89\)90007-0](https://doi.org/10.1016/0264-3707(89)90007-0)
- 748 Cowie, L., & Kuszniir, N. (2012). Mapping crustal thickness and oceanic lithosphere
749 distribution in the Eastern Mediterranean using gravity inversion. *Petroleum*
750 *Geoscience, 18*(4), 373–380. <https://doi.org/10.1144/petgeo2011-071>
- 751 Dart, C. J., Bosence, D. W., & McClay, K. R. (1993). Stratigraphy and structure of the Maltese
752 graben system. *Journal of the Geological Society, London, 150*, 1153–1166.
- 753 Dewey, J. F., Helman, M. L., Knott, S. D., Turco, E., & Hutton, D. H. W. (1989). Kinematics of
754 the western Mediterranean. *Geological Society Special Publication, 45*, 265–283.
755 <https://doi.org/10.1144/GSL.SP.1989.045.01.15>
- 756 Doglioni, C. (2024). Gravitational and elastic energies stored in crustal volumes activate
757 normal versus strike-slip and thrust seismogenic faults. *Geoscience Frontiers, 15*(6),
758 101894. <https://doi.org/10.1016/j.gsf.2024.101894>
- 759 Dunham, R. J. (1962). Classification of carbonate rocks according to depositional texture. In
760 W. E. Ham (Ed.), *Classification of carbonate rocks* (pp. 108–121). Mem. Am. Ass. Petrol.
761 Geol.
- 762 Embry, A. F., & Klovan, J. E. (1971). A Late Devonian reef tract on northeastern Banks Island,
763 Northwest Territories. *Bull. Can. Petrol. Geol., 58*, 730–781.

- 764 Faccenna, C., Piromallo, C., Crespo-Blanc, A., Jolivet, L., & Rossetti, F. (2004). Lateral slab
765 deformation and the origin of the western Mediterranean arcs. *Tectonics*, 23(1).
766 <https://doi.org/10.1029/2002TC001488>
- 767 Felix, R. (1973). *Oligo-Miocene stratigraphy of Malta and Gozo* (Vols 73–20). Veeman &
768 Zonen.
- 769 Finetti, I. (1982). Structure, stratigraphy and evolution of the Central Mediterranean.
770 *Bollettino Di Geofisica Teorica Ed Applicata*, XXIV(96), 247–312.
- 771 Galea, P. (2007). Seismic history of the Maltese Islands and considerations on seismic risk.
772 *Annals of Geophysics*, 50, 725–740.
- 773 Gallais, F., Gutscher, M. A., Graindorge, D., Chamot-Rooke, N., & Klaeschen, D. (2011). A
774 Miocene tectonic inversion in the Ionian Sea (central Mediterranean): Evidence from
775 multichannel seismic data. *Journal of Geophysical Research: Solid Earth*, 116(12).
776 <https://doi.org/10.1029/2011JB008505>
- 777 Gardiner, W., Grasso, M., & Sedgeley, D. (1995). Plio-Pleistocene fault movement as
778 evidence for mega-block kinematics within the Hylean-Malta Plateau, Central
779 Mediterranean. *J. Geodynamics*, 19(1), 5–51.
- 780 Gatt, P. (2005). Syntectonic deposition of an Oligo-Miocene phosphorite conglomerate bed
781 in Malta. *The Central Mediterranean Naturalist*, 4(2), 109–118.
- 782 Gatt, P. (2007). Controls on Plio-Quaternary foreland sedimentation in the region of the
783 Maltese Islands. *Bollettino Della Societa Geologica Italiana*, 126(1), 119–129.
- 784 Gatt, P. (2012). *Carbonate facies, depositional sequences and tectonostratigraphy of the*
785 *Paleogene Malta Platform* [Unpublished PhD thesis, University of Durham, UK].
786 <https://etheses.dur.ac.uk/4425/>
- 787 Gatt, P. (2019). Evaporite dissolution sinkholes in the Dwejra Depression, Malta. *Eur Geol*,
788 48, 53–57.
- 789 Gatt, P. (2022). Facies, depositional environments and drowning of Tethyan isolated
790 carbonate platforms: the Paleogene carbonates of Malta. *Facies*, 68(3), 9.
791 <https://doi.org/10.1007/s10347-022-00648-1>
- 792 Gatt, P. (2025). Tectonic segmentation of the Mesozoic to Paleogene Malta Isolated
793 Carbonate Platform: A key to rifting in the Central Mediterranean. *Tectonics*, 44,
794 e2025TC008902. <https://doi.org/10.1029/2025TC008902>
- 795 Gatt, P. A. (2006). Model of limestone weathering and damage in masonry:
796 Sedimentological and geotechnical controls in the Globigerina Limestone Formation
797 (Miocene) of Malta. *Xjenza*, 11, 30–39.
- 798 Gatt, P., Tucker, M., & Davies, R. (2009). Drowning of the Malta carbonate platform: facies
799 and sequence stratigraphy of the Lower Coralline Limestone (U. Oligocene) . In Pascucci

- 800 V & Andreucci S (Eds.), *Sedimentary environments of Mediterranean islands* (p. 181).
801 Inter. Assoc. of Sedimentologists.
- 802 Goes, S., Jenny, S., Hollenstein, C., Kahle, H. G., & Geiger, A. (2004). A recent tectonic
803 reorganization in the south-central Mediterranean. *Earth and Planetary Science Letters*,
804 226(3–4), 335–345. <https://doi.org/10.1016/j.epsl.2004.07.038>
- 805 Grasso, M., & Pedley, H. M. (1985). The Pelagian Islands: A new geological interpretation
806 from sedimentological and tectonic studies and its bearing on the evolution of the
807 Central Mediterranean (Pelagian block). *Geologica Rom.*, 24, 13–34.
- 808 Grasso, M., Reuther, C-D, Baumann, H, & Becker, A. (1986). Shallow crustal stress and
809 neotectonic framework of the Malta platform and the southeastern Pantelleria Rift
810 (Central Mediterranean). *Geologica Rom.*, 25, 191–212.
- 811 Guiraud, R., & Bosworth, W. (1999). Phanerozoic geodynamic evolution of northeastern
812 Africa and the northwestern Arabian platform. In *Tectonophysics* (Vol. 315).
813 www.elsevier.com/locate/tecto
- 814 Gutscher, M. A., Kopp, H., Krastel, S., Bohrmann, G., Garlan, T., Zaragosi, S., Klaucke, I.,
815 Wintersteller, P., Loubrieu, B., Le Faou, Y., San Pedro, L., Dominguez, S., Rovere, M.,
816 Mercier de Lepinay, B., Ranero, C., & Sallares, V. (2017). Active tectonics of the
817 Calabrian subduction revealed by new multi-beam bathymetric data and high-
818 resolution seismic profiles in the Ionian Sea (Central Mediterranean). *Earth and*
819 *Planetary Science Letters*, 461, 61–72. <https://doi.org/10.1016/j.epsl.2016.12.020>
- 820 Gutscher, M. A., Roger, J., Baptista, M. A., Miranda, J. M., & Tinti, S. (2006). Source of the
821 1693 Catania earthquake and tsunami (southern Italy): New evidence from tsunami
822 modeling of a locked subduction fault plane. *Geophysical Research Letters*, 33(8).
823 <https://doi.org/10.1029/2005GL025442>
- 824 Harrison, J. C. (1954). Gravity measurement on Malta and Tunis. *Geophysical Journal*
825 *International*, 6, 604–609. <https://doi.org/10.1111/j.1365-246X.1954.tb03043.x>
- 826 Hilgen, F. J., Abels, H. A., Iaccarino, S., Krijgsman, W., Raffi, I., Sprovieri, R., Turco, E., &
827 Zachariasse, W. J. (2009). The Global Stratotype Section and Point (GSSP) of the
828 Serravallian Stage (Middle Miocene). *Episodes*, 32(3), 152–166.
829 <https://doi.org/10.18814/epiiugs/2009/v32i3/002>
- 830 Hollenstein, Ch., Kahle, H. -G., Geiger, A., Jenny, S., Goes, S., & Giardini, D. (2003). New GPS
831 constraints on the Africa-Eurasia plate boundary zone in southern Italy. *Geophysical*
832 *Research Letters*, 30(18). <https://doi.org/10.1029/2003GL017554>
- 833 Hsu, K., Ryan, W., & Cita, M. (1973). Late Miocene dessication of the Mediterranean.
834 *Nature*, 242, 240–244.
- 835 Illies, J. H. (1981). Graben formation - the Maltese Islands, a case history. *Tectonophysics*,
836 73, 151–168.
- 837 INGV. (2025). <https://terremoti.ingv.it/en>. <https://terremoti.ingv.it/en>

- 838 Jolivet, L., & Faccenna, C. (2000). Mediterranean extension and the Africa-Eurasia collision.
839 *Tectonics*, 19(6), 1095–1106. <https://doi.org/10.1029/2000TC900018>
- 840 Jongsma, D., van Hinte, J. E., & Woodside, J. M. (1985). Geologic structure and neotectonics
841 of the North African continental margin south of Sicily. *Mar Pet Geol*, 2(2), 156–179.
842 [https://doi.org/10.1016/0264-8172\(85\)90005-4](https://doi.org/10.1016/0264-8172(85)90005-4)
- 843 Jongsma, D., Woodside, J. M., King, G. C. P., & Van Hinte, J. E. (1987). The Medina Wrench: a
844 key to the kinematics of the central and eastern Mediterranean over the past 5 Ma.
845 *Earth and Planetary Science Letters*, 82, 87–106.
- 846 Krijgsman, W., Hilgen, F. J., Raffi, I., Sierro, F. J., & Wilson, D. S. (1999). Chronology, causes
847 and progression of the Messinian salinity crisis. *Nature*, 400, 652–655.
848 www.nature.com
- 849 Letouzey, J., Colletta, B., & Chermette, J. C. (1995). Evolution of Salt-Related Structures in
850 Compressional Settings. In M. Jackson, D. G. Roberts, & S. Snelson (Eds.), *Salt Tectonics:
851 A Global Perspective* (pp. 41–60). AAPG Memoir 65.
852 <https://archives.datapages.com/data/specpubs/memoir65/ch03/0041.htm>
- 853 Maiorana, M., Artoni, A., Le Breton, E., Sulli, A., Chizzini, N., & Torelli, L. (2023). Is the Sicily
854 Channel a simple Rifting Zone? New evidence from seismic analysis with geodynamic
855 implications. *Tectonophysics*, 864. <https://doi.org/10.1016/j.tecto.2023.230019>
- 856 Malinverno, A., & Ryan, W. B. F. (1986). Extension in the Tyrrhenian Sea and shortening in
857 the Apennines as result of arc migration driven by sinking of the lithosphere. *Tectonics*,
858 5(2). <https://doi.org/10.1029/TC005i002p00227>
- 859 Marriner, N., Gambin, T., Djamali, M., Morhange, C., & Spiteri, M. (2012). Geoarchaeology of
860 the Burmarrad ria and early Holocene human impacts in western Malta.
861 *Palaeogeography, Palaeoclimatology, Palaeoecology*, 339–341, 52–65.
862 <https://doi.org/10.1016/j.palaeo.2012.04.022>
- 863 Martinelli, M., Bistacchi, A., Balsamo, F., & Meda, M. (2019). Late Oligocene to Pliocene
864 extension in the Maltese Islands and implications for geodynamics of the Pantelleria
865 Rift and Pelagian Platform. *Tectonics*, 38(9), 3394–3415.
866 <https://doi.org/10.1029/2019TC005627>
- 867 Miller, K. G., Browning, J. V., Schmelz, W. J., Kopp, R. E., Mountain, G. S., & Wright, J. D.
868 (2020). *Cenozoic sea-level and cryospheric evolution from deep-sea geochemical and
869 continental margin records*. <https://www.science.org>
- 870 Miller, K. G., Kominz, M. A., Browning, J. V., Wright, J. D., Mountain, G. S., Katz, M. E.,
871 Sugarman, P. J., Cramer, B. S., Christie-Blick, N., & Pekar, S. F. (2005). The Phanerozoic
872 record of global sea-level change. In *Science* (Vol. 310, Issue 5752, pp. 1293–1298).
873 <https://doi.org/10.1126/science.1116412>
- 874 Moody, J. D., & Hill, M. J. (1956). Wrench-fault tectonics. *GSA Bulletin*, 67(9), 1207–1246.
875 [https://doi.org/10.1130/0016-7606\(1956\)67\[1207:WT\]2.0.CO;2](https://doi.org/10.1130/0016-7606(1956)67[1207:WT]2.0.CO;2)

- 876 Nocquet, J.-M. (2012). Present-day kinematics of the Mediterranean: A comprehensive
877 overview of GPS results. *Tectonophysics*, 579, 220–242.
878 <https://doi.org/10.1016/j.tecto.2012.03.037>
- 879 Palano, M., Ursino, A., Spampinato, S., Sparacino, F., Polonia, A., & Gasperini, L. (2020).
880 Crustal deformation, active tectonics and seismic potential in the Sicily Channel
881 (Central Mediterranean), along the Nubia–Eurasia plate boundary. *Scientific Reports*,
882 10(1). <https://doi.org/10.1038/s41598-020-78063-1>
- 883 Pedley, H. M. (1978). A new lithostratigraphical and palaeoenvironmental interpretation for
884 the coralline limestone formations (Miocene) of the Maltese Islands. *Overseas Geol. &*
885 *Miner. Resour.*, 54, 1–17.
886 [https://pubs.bgs.ac.uk/publications.html?pubID=B03990#f=true&v=d&z=2&n=5&i=B03](https://pubs.bgs.ac.uk/publications.html?pubID=B03990#f=true&v=d&z=2&n=5&i=B03990_0011.jp2&y=750&x=306)
887 [990_0011.jp2&y=750&x=306](https://pubs.bgs.ac.uk/publications.html?pubID=B03990#f=true&v=d&z=2&n=5&i=B03990_0011.jp2&y=750&x=306)
- 888 Pedley, H. M., & Grasso, M. (1992). Miocene syntectonic sedimentation along the western
889 margins of the Hyblean-Malta platform: A guide to plate margin processes in the
890 central Mediterranean. *J. Geodynamics*, 15(1), 19–37.
- 891 Pedley, H. M., House, M. R., & Waugh, B. (1976). The geology of Malta and Gozo.
892 *Proceedings of the Geologists' Association*, 87(3), 325–341.
893 [https://doi.org/10.1016/S0016-7878\(76\)80005-3](https://doi.org/10.1016/S0016-7878(76)80005-3)
- 894 Pedley, H. M., House, M. R., & Waugh, B. (1978). The geology of the Pelagian Block: The
895 Maltese Islands. In A. E. M. Nairn, W. H. Kanes, & F. G. Stehli (Eds.), *The Ocean Basins*
896 *and margins* (pp. 417–433). Plenum Press.
- 897 Pedley, M. (2011). The Calabrian stage, Pleistocene highstand in Malta: A new marker for
898 unravelling the Late Neogene and Quaternary history of the islands. *Journal of the*
899 *Geological Society*, 168(4), 913–926. <https://doi.org/10.1144/0016-76492010-080>
- 900 Putz-Perrier, M. W., & Sanderson, D. J. (2010). Distribution of faults and extensional strain in
901 fractured carbonates of the North Malta Graben. *American Association of Petroleum*
902 *Geologists Bulletin*, 94(4), 435–456. <https://doi.org/10.1306/08260909063>
- 903 Ragg, S., Grasso, M., & Müller, B. (1999). Patterns of tectonic stress in Sicily from borehole
904 breakout observations and finite element modeling. *Tectonics*, 18(4), 669–685.
905 <https://doi.org/10.1029/1999TC900010>
- 906 Reuther C.D. (1984). Tectonics of the Maltese Islands. *Centro*, 1, 1–20.
- 907 Reuther, C.-D., & Eisbacher, G. H. (1985). Pantelleria Rift-crustal extension in a convergent
908 intraplate setting. *Geologische Rundschau*, 74(3), 585–597.
- 909 Ricou, L. E. (1994). La thétys reconstruite: plaques, blocs continentaux et leurs limites depuis
910 260 ma de l'amérique centrale à l'asie du sud-est. *Geodinamica Acta*, 7(4), 169–218.
911 <https://doi.org/10.1080/09853111.1994.11105266>
- 912 Rosenbaum, G. (2014). Geodynamics of oroclinal bending: Insights from the Mediterranean.
913 *Journal of Geodynamics*, 82, 5–15. <https://doi.org/10.1016/j.jog.2014.05.002>

- 914 Rosenbaum, G., Lister, G. S., & Duboz, C. (2002). Relative motions of Africa, Iberia and
 915 Europe during Alpine orogeny. *Tectonophysics*, 359, 117–129.
 916 www.elsevier.com/locate/tecto
- 917 Roure, F., Casero, P., & Addoum, B. (2012). Alpine inversion of the North African margin and
 918 delamination of its continental lithosphere. *Tectonics*, 31(3).
 919 <https://doi.org/10.1029/2011TC002989>
- 920 Roveri, M., Flecker, R., Krijgsman, W., Lofi, J., Lugli, S., Manzi, V., Sierro, F. J., Bertini, A.,
 921 Camerlenghi, A., De Lange, G., Govers, R., Hilgen, F. J., Hübscher, C., Meijer, P., &
 922 Stoica, M. (2014). The Messinian Salinity Crisis: Past and future of a great challenge for
 923 marine sciences. *Marine Geology*, 352, 25–58.
 924 <https://doi.org/10.1016/j.margeo.2014.02.002>
- 925 Rusciadelli, G., & Shiner, P. (2018). Isolated carbonate platforms of the Mediterranean and
 926 their seismic expression—searching for a paradigm. *Leading Edge*, 37(7), 492–501.
 927 <https://doi.org/10.1190/tle37070492.1>
- 928 Serpelloni, E., Cavaliere, A., Martelli, L., Pintori, F., Anderlini, L., Borghi, A., Randazzo, D.,
 929 Bruni, S., Devoti, R., Perfetti, P., & Cacciaguerra, S. (2022). Surface velocities and strain-
 930 rates in the Euro-Mediterranean region from massive GPS data processing. *Frontiers in*
 931 *Earth Science*, 10. <https://doi.org/10.3389/feart.2022.907897>
- 932 Serpelloni, E., Vannucci, G., Pondrelli, S., Argnani, A., Casula, G., Anzidei, M., Baldi, P., &
 933 Gasperini, P. (2007). Kinematics of the Western Africa-Eurasia plate boundary from
 934 focal mechanisms and GPS data. *Geophysical Journal International*, 169(3), 1180–1200.
 935 <https://doi.org/10.1111/j.1365-246X.2007.03367.x>
- 936 Serra-Kiel, J., Hottinger, L., Esmeralda, C., Drobne, K., Ferrandez, C., Jauhri, A. J., Less, G.,
 937 Pavlovec, R., Pignatti, J., Samsó, J. M., Schaub, H., Sirel, E., Strougo, A., Tambareau, Y.,
 938 Tosquella, J., & Zakrevskaya, E. (1998). Larger foraminiferal biostratigraphy of the
 939 Tethyan Paleocene and Eocene. *Bull. Soc. Geol. France*, 169(2), 281–299.
- 940 Sibson, R. H. (1995). Selective fault reactivation during basin inversion: Potential for fluid
 941 redistribution through fault-valve action. *Geological Society Special Publication*, 88, 3–
 942 19. <https://doi.org/10.1144/GSL.SP.1995.088.01.02>
- 943 Soumaya, A., Ben Ayed, N., Delvaux, D., & Ghanmi, M. (2015). Spatial variation of present-
 944 day stress field and tectonic regime in Tunisia and surroundings from formal inversion
 945 of focal mechanisms: Geodynamic implications for central Mediterranean. *Tectonics*,
 946 34(6), 1154–1180. <https://doi.org/10.1002/2015TC003895>
- 947 Speranza, F., Hernandez-Moreno, C., Avellone, G., Gasparo Morticelli, M., Agate, M., Sulli,
 948 A., & Di Stefano, E. (2018). Understanding Paleomagnetic Rotations in Sicily: Thrust
 949 Versus Strike-Slip Tectonics. *Tectonics*, 37(4), 1138–1158.
 950 <https://doi.org/10.1002/2017TC004815>

- 951 Speranza, F., Minelli, L., Pignatelli, A., & Chiappini, M. (2012). The Ionian Sea: The oldest in
 952 situ ocean fragment of the world? *Journal of Geophysical Research: Solid Earth*,
 953 117(12). <https://doi.org/10.1029/2012JB009475>
- 954 Sulli, A., Gasparo Morticelli, M., Agate, M., & Zizzo, E. (2021). Active north-vergent thrusting
 955 in the northern Sicily continental margin in the frame of the quaternary evolution of
 956 the Sicilian collisional system. *Tectonophysics*, 802, 228717.
 957 <https://doi.org/10.1016/j.tecto.2021.228717>
- 958 Sylvester, A. (1988). Strike-slip faults. *Bulletin of the Geological Society of America*, 100(11),
 959 1666–1703. [https://doi.org/10.1130/0016-7606\(1988\)100<1666:SSF>2.3.CO;2](https://doi.org/10.1130/0016-7606(1988)100<1666:SSF>2.3.CO;2)
- 960 Tchalenko, J. S. (1970). Similarities between shear zones of different magnitudes. *Bulletin of*
 961 *the Geological Society of America*, 81(6), 1625–1640. [https://doi.org/10.1130/0016-](https://doi.org/10.1130/0016-7606(1970)81[1625:SBSZOD]2.0.CO;2)
 962 [7606\(1970\)81\[1625:SBSZOD\]2.0.CO;2](https://doi.org/10.1130/0016-7606(1970)81[1625:SBSZOD]2.0.CO;2)
- 963 Tugend, J., Chamot-Rooke, N., Arsenikos, S., Blanpied, C., & Frizon de Lamotte, D. (2019).
 964 Geology of the Ionian Basin and Margins: A Key to the East Mediterranean
 965 Geodynamics. *Tectonics*, 38(8), 2668–2702. <https://doi.org/10.1029/2018TC005472>
- 966 van Dijk, J. P., & Scheepers, P. J. J. (1995). Neotectonic rotations in the Calabrian Arc;
 967 implications for a Pliocene-Recent geodynamic scenario for the Central Mediterranean.
 968 *Earth-Science Reviews*, 39, 207–246.
- 969 van Hinsbergen, D. J. J., Torsvik, T. H., Schmid, S. M., Mañenco, L. C., Maffione, M., Vissers, R.
 970 L. M., Gürer, D., & Spakman, W. (2020). Orogenic architecture of the Mediterranean
 971 region and kinematic reconstruction of its tectonic evolution since the Triassic.
 972 *Gondwana Research*, 81, 79–229. <https://doi.org/10.1016/j.gr.2019.07.009>
- 973 Vossmerbaumer, H. (1972). *Malta: ein Beitrag zur Geologie und Geomorphologie des*
 974 *Zentral-Mediterranean Raumes*. Wurzbürger Geographische Arbeiten 38.
- 975 Wardell Armstrong. (1996). *Mineral Resources Assessment for the Planning Authority of*
 976 *Malta*.
- 977 Zoback, M. Lou. (1992). First-and Second-Order Patterns of stress in the lithosphere: The
 978 world stress map project. *Journal of Geophysical Research*, 97, 11703–11728.
 979 <https://digitalcommons.unl.edu/usgsstaffpub/461>
- 980 Zwaan, F., Schreurs, G., Buitter, S. J. H., Ferrer, O., Reitano, R., Rudolf, M., &
 981 Willingshofer, E. (2022). Analogue modelling of basin inversion: a review and
 982 future perspectives. *Solid Earth*, 13(12), 1859–1905. [https://doi.org/10.5194/se-](https://doi.org/10.5194/se-13-1859-2022)
 983 [13-1859-2022](https://doi.org/10.5194/se-13-1859-2022)

984

985

986 **Figure captions**

987 **Fig. 1.** Dashed yellow line shows extent of carbonate platforms: MICP and HP
988 (Hyblean carbonate platform) in the Central Mediterranean. (a) Main geotectonic
989 features marked by the circled numbers: 1. Hyblean-Malta Plateau (HMP) bounded on
990 the south by the Medina Wrench (S3) and on the west by the Scicli Fault (S1), 2. Gela
991 Basin (foredeep) bound on the west by the Sciacca Fault (S2), 3. Ionian crust overlain
992 by accretionary prism, 4. Sicilian-Maghrebian thrust belt, 5. Calabrian Arc, 6.
993 Pantelleria Rift and main grabens: Pantelleria Graben (PG) separated by the Sciacca
994 Fault (S2) from the Linosa Graben (LG), Malta Graben (MG) and the Medina Trough
995 (MT), 7. Ionian oceanic crust. (b) Maltese Islands: North Gozo Graben (NGG), North
996 Malta Graben (NMG), location of seismic lines 1 to 6, main faults (in red) and wells
997 mentioned in the text, (c) Cross section A-A' along the Cenozoic foreland succession
998 of the Malta Horst (legend for lithology in Fig. 2), (d) Generalised NW-SE cross-section
999 along Malta Horst showing influence of WMP basement on thrusting (no erosion
1000 shown). Stratigraphy based on MTZ and NAX wells.

1001 **Fig. 2.** Stratigraphy of the MICP. (a) Stratigraphy of the MICP. (b) Seismic velocity and
1002 main reflectors around the AQU well. (c) Cenozoic stratigraphy of MICP. (d) Global
1003 sea level curve based on Miller et al. (2020) and tectonic phases A to E. Dotted green
1004 line shows relative sea level in Malta Horst, (e) Plio-Quaternary eustacy (Miller et al.,
1005 2005) and stratigraphy, (f) timing of growth of Malta Graben (MG), North Malta Graben
1006 (NMG), North Gozo Graben (NGG) and Marsascula Anticline (MA), Valletta Anticline
1007 (VA), Naxxar Anticline (NA).

1008 **Fig. 3.** Tectonic phases A to D: (a) Seismic line 1 showing undeformed Naxxar Basin
1009 (phase A), (b) Palaeomap showing the West Malta Palaeohigh (WMP) and the growth
1010 of the Naxxar and Valletta basins (phase A) and Marsaxlokk Basin (phase B), (c)
1011 Phase D NW and NE trending faulting by N-S extension, (d) Palinspastic
1012 reconstruction of cross section C-C' showing development of basins in phases A and
1013 B, (e) Phase E faulting and Areas 1 to 4. Square dots are earthquakes occurring in
1014 2015 (Bozionelos et al, 2017), (f) Models of deformation during phases A, D and E.

1015 **Fig. 4.** Map of Areas 1, 2, 3 and 4 and location of seismic lines 2 to 6. (a) Interpreted
1016 and uninterpreted seismic line in Area 1. (b) Seismic line 2 showing thrusts that sole
1017 along E1 gypsum bed. Seismic line 3 showing relay ramp produced during Phase D.
1018 (c) Seismic line 5 showing negative flower structure over Hurd bank Fault and positive
1019 flower structure over Maghlaq Fault, (d) Positive flower structure over West Malta Fault
1020 (b, c, and d same scale).

1021 **Fig. 5.** (a) Phase E compressive deformation in Area 1: 1. Marsascula Anticline, 2.
1022 Zabbar Anticline, 3. Valletta Anticline. 4. Naxxar Anticline, 5. Ghallis Anticline, 6.
1023 Marsaxlokk Syncline, 7. San Leonardo Syncline infilled with Calabrian carbonates, 8-
1024 9. Sliema-Hamrun Syncline, 10. Pieta Anticline, 11. Mqabba Basin (Area 2); (b) Inset

1025 of Area 1 showing topography and dip of beds and location of Wied il-Ghasel
1026 palaeoriver mentioned in text. The orientation of S_H max is from Grasso et al., 1986;
1027 (c) Inset showing left-lateral strike-slip faults along Mellieha Ridge and Bugibba (Area
1028 4), (d) South Gozo Fault dextral strike-slip fault showing anticline (compression) on
1029 west and feather structures (extension) along east.

1030 **Fig. 6.** Cross sections, outcrops and borehole data (locations shown in map). (a) Cross
1031 section a-a' showing five Oligo-Miocene formations in Malta, (b) Cross section b-b'
1032 showing inversion tectonics along NE coast of Malta (top cross section has no vertical
1033 exaggeration). Thrusts 1 to 6 shown, (c) Cross section c-c' of crest of Zabbar Anticline
1034 with TD2 exposed, (d) Cross section d-d' through Hamrun-Sliema syncline, (e and f)
1035 Cross-sections e-e' and f-f' through Naxxar Anticline, (g) Stratigraphic logs of
1036 boreholes and outcrops A to I, (h) Photograph of erosion along margin of Naxxar Fault
1037 footwall close to locality D, (i) Series of faults synthetic to Valletta Fault close to locality
1038 H. (j) Map of cross sections and outliers.

1039 **Fig. 7.** The Wied Faham Overthrust (denoted by X) within the Naxxar Anticline: (a)
1040 Map showing location of overthrust in relation of Great Fault, (b) Lithology of Wied
1041 Faham Overthrust with accompanying photographs: (i) the 15° dip of floor thrust
1042 exposed along road cut, (ii) the 10° dip of roof thrust along Wied Faham and (iii)
1043 antithetic faults to the Great Fault draped with Blue Clay adjacent to the overthrust X.
1044 (c) Cross section of overthrust X interpreted as an overturned fold that downflexed the
1045 hangingwall of the Great Fault. The loading of the hanging wall of Great Fault
1046 preserved an outlier of Upper Globigerina Limestone (TH) with clay (TI).

1047 **Fig. 8.** Regional geodynamics and deformation by Africa-Eurasia convergence
1048 (arrows marked σ_1) (Hollenstein et al., 2003): (a) Foreland deformation of the Malta
1049 Horst: First order Master faults (122°N) that bound the Malta Horst are shown in red;
1050 2nd order in blue and 3rd order deformations in green. Areas 1 to 4 based on this
1051 study, Area 5 is based on Gardiner et al., 1995. Round dots are earthquakes (data
1052 from INGV), (b) Strain ellipse, (c) Schematic development of the Pantelleria Rift
1053 grabens along the Medina Wrench (based on Jongsma et al., 1987), (d) Compression
1054 and extension around the Maltese Islands.

1055